Published in final edited form as:
Colloids Surf A Physicochem Eng Asp. 2019 April 5; 566: 188–195. doi:10.1016/j.colsurfa.2019.01.026.

Improved reductive transformation of iopromide by magnetite containing reduced graphene oxide nanosacks as electron shuttles

E. Toral-Sánchez[1], **Robert H. Hurt**[2], **Juan A. Ascacio Valdés**[3], **Cristóbal N. Aguilar**[3], **F.J. Cervantes**[1], **J.R. Rangel-Mendez**[1]

[1]IPICYT/División de Ciencias Ambientales. Camino a la Presa San José 2055, Col. Lomas 4a. Sección, C.P. 78216, San Luis Potosí, SLP, México.

[2]School of Engineering/Institute for Molecular and Nanoscale Innovation (IMNI), Brown University, Providence, Rhode Island 02912, United States.

[3]Food Research Department, School of Chemistry (DIA-UAdeC), Universidad Autónoma de Coahuila. Saltillo, 25280, Coahuila, México.

Abstract

The novel application of magnetite containing reduced graphene oxide nanosacks (MrGO-N) as electron shuttles to improve the reductive degradation of pharmaceutical pollutant, iopromide (IOP), was evaluated. The MrGO-N were synthesized by ultrasonicated nebulization process, and their physicochemical characterization was performed by potentiometric titrations, zeta potential, high resolution transmission electron microscopy (HR-TEM), X-ray diffraction, as well as by Raman and Fourier transform infrared spectroscopies. Results demonstrated the thermal reduction of precursor graphene oxide sheets, the removal of different oxygenated groups, and the successful assembly of magnetite nanoparticles (MNP) in the graphene sacks. Also, reduction experiments revealed 72 % of IOP removal efficiency and up to 2.5-fold faster degradation of this pollutant performed with MrGO-N as redox catalysts in batch assays and with sulfide as electron donor. Chemical transformation pathway of IOP provides evidence of complete dehalogenation and further transformation of aromatic ring substituents. Greater redox-mediating ability of MrGO-N was observed, which was reflected in the catalytic activity of these nanomaterials during the reductive degradation of IOP. Transformation byproducts with simpler chemical structure were identified, which could lead to complete degradation by conventional methodologies in a complementary treatment process. Redox-mediating activity of MrGO-N could potentially be applied in wastewater treatment systems in order to facilitate the biodegradation of priority contaminants.

Graphical Abstract

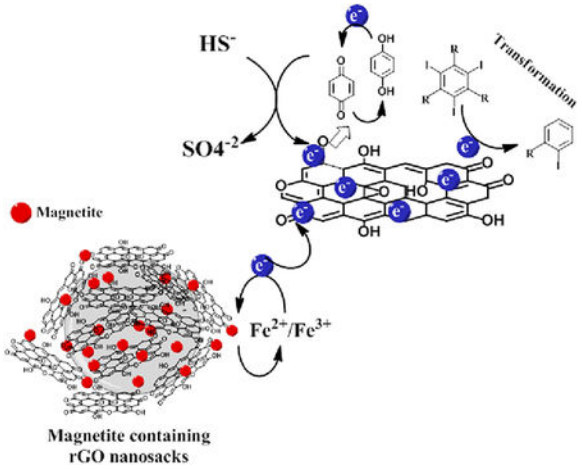

Keywords

Reductive transformation; iopromide; graphene nanosacks; electron shuttle; X-ray contrast medium

1. Introduction

Recently, many emerging pollutants like pharmaceuticals have been identified in effluents from wastewater treatments (WWT) systems and aquatic environments around the world. Iopromide (IOP) is a tri-iodinated X-ray contrast medium (ICM) frequently used in radiographic tests, which is eliminated by urine in the first 24 h [1,2]. Because of its low microbial degradation and physicochemical properties, IOP is considered as a persistent pollutant that is resistant to conventional WWT and consequently discharged into environmental compartments like water bodies and soils [1,3,4]. IOP has been detected in effluents from WWT plants, receiving water bodies, and even treated tap water at μg/L levels [5,6]. Although no adverse effects have been documented on the chronic exposure of this pollutant [7], different studies have reported toxic effects at cellular level conducting to apoptosis and endothelial disfunction [8–10]. In addition, it has been documented that exposure to ICM leads to damage to human health include allergic reactions, cardiac problems and systemic manifestations [11]. Therefore, it is essential to develop new degradation strategies as an alternative to remove of this halogenated organic compound from polluted effluents.

Several researches have studied the degradation of priority pollutants by the use of chemical substances that have the ability to serve as redox catalysts, mainly attributed to the presence of quinone groups (two resonant carbonyl groups[12]), which form a well-known redox couple with hydroquinones that facilitate system electron transfer [13]. Quinone-hydroquinone couples are the perfect case of electron shuttle systems, and their redox-mediator nature consist in the capacity to accept and donate electrons by resonance phenomenon [12,14]. Some graphene based-materials like graphene oxide (GO), reduced graphene oxide (rGO) and graphene composites have also been applied as electron shuttle with rapid electron transfer capacity and redox-mediating activity [15–17], possibly due to

the presence of carbonyl groups in the population of diverse oxygen-containing groups on these complex materials [18–20]. Moreover, it has been well supported that the π-electrons located in the zigzag edges of graphene sheets exhibit excellent catalytic activity, desired selectivity and chemical stability, serving as catalysts in the electron transfer reactions [21].

Recently, it has been explored the catalytic performance of GO-based materials in the redox conversion of environmental contaminants because of their ability to improve the electron transfer process by complex physicochemical mechanisms [18]. For instance, Colunga et al., [22] and Lu et al., [23] reported the reduction of azo dyes using GO-based materials as catalysts. Also, Fu et al., [24] studied the reductive transformation of polyhalogenated organics. Meanwhile, several authors have documented the redox conversion of nitrocompounds [18,25]. In addition, our previous work has proved that GO and rGO can act as redox catalysts, facilitating the chemical/biological degradation of IOP in batch incubations and using sulfide as electron donor [26,27]. There is significant evidence that GO-based materials can promote reductive reactions of persistent pollutants like halogenated organics, but their application in continuous treatment systems is hindered by challenges in capturing and recovering the mediator after use. An important goal is to design graphene-based composite mediators with specific properties that allow them to be retained or captured, and recycled back into treatment processes.

Recently, the immobilization of particles in graphene structures has emerged as a new approach to produce versatile hybrid carbon nanomaterials with specific properties and functions [28]. In this context, different alternatives have been studied about iron containing graphene structures. Panich et al., [29] reported the structure and magnetic properties of iron (Fe^{2+}/Fe^{3+}) ions-doped micro- and nanosized graphene flakes, concluding that the Fe ions are attached in the edges of graphene sheets by oxygen functional groups and atomic hydrogen. On the other hand, an aerosol-phase process has been reported for the assembly of nanoparticles and rGO sheets in the form of filled graphene nanosacks (GNS) by fast microdroplet drying [28]. Nowadays, several studies have reported the use of magnetite nanoparticles (MNP), especially magnetite (Fe_3O_4), in environmental and medical biotechnology, removal of water pollutants and catalysis research area, due to their particular properties, such as high surface area, superparamagnetism and reducing catalytic power [30]. Recently, the integration of MNP in hybrid GNS has been demonstrated, and their application in biomedical and chemical technologies has also been studied [28,31]. However, their redox catalytic properties to facilitate the reductive degradation of recalcitrant pollutants in water have not been explored yet. In addition, the presence of MNP in the hybrid GNS implies that the reductive transformation mechanisms of pollutants are more complex than those involved in the presence of GO-based materials as electron shuttles. Accordingly, it is important to study the redox performance of MrGO-N for future applications in the transformation of priority contaminants.

The aim of this study was to evaluate the novel use of magnetite containing reduced graphene oxide nanosacks (MrGO-N) as electron shuttle to promote reductive transformation reactions of IOP in chemical systems. The experimental work is conducted in batch incubations, but the goal is to develop and demonstrate the magnetic function that would allow application in biological continuous systems with magnetic recovery. Moreover,

the influence of the physical and chemical properties of the MrGO-N in the capacity to serve as electron shuttles is studied as are the transformation pathways for abiotic reduction of IOP in these systems.

2. Materials and methods

2.1. Materials and chemicals

IOP (Ultravist® 370) was purchased from Bayer Schering Pharma. Sodium sulfide ($Na_2S{\cdot}9H_2O$) and magnetite nanoparticles (Fe_3O_4, particle size of <50 nm) were obtained from Fisher-Scientific and Sigma Aldrich, respectively, with 99% purity. The basal medium (pH = 7.6) and trace elements solution (1 mL/L) used in chemical reduction experiments were mixtures of several reagents as described in previous works,[19,26,27,32] All solutions were prepared with deionized (DI) water to 18.1 MΩ·cm. GO aqueous suspensions were prepared and purified by a modified Hummers' method as described previously [33].

2.2. Synthesis of magnetite containing graphene oxide nanosacks

The fabrication of MrGO-N was carried out by ultrasonicated nebulization process using a well-mixed colloidal suspension of GO (0.5 mg/mL) and Fe_3O_4 nanoparticles (1 mg/mL), according to methodology previously proposed [28,31]. The MrGO-N were recovered on a filter membrane and dispersed in DI water. Hybrid rGO nanosacks without magnetite (rGO-N) were similarly synthesized to MrGO-N as mentioned above.

2.3. Characterization of graphene nanosacks

Morphological characterization of MrGO-N and rGO-N was performed on a LEO 1530 VP Scanning Electron Microscope (SEM) and JEOL JEM-2010 High Resolution Transmission Electron Microscope (HRTEM). Samples were suspended in ethanol and then sonicated for 30 min. After that, the samples were mounted in a Cu TEM grid. Raman spectroscopy was performed on a WITEC-A300M+ Confocal Raman Microscope with laser frequency of 514 nm as excitation source trough a 50× objective. Zeta potential measurements of the samples were measured in DI water using a Malvern Nano-ZS dynamic light scattering equipment. X-ray diffraction (XRD) patterns were obtained in a Bruker D8 Advanced diffractometer using CuKα radiation. Infrared spectra were recorded by Fourier transform-infrared (FT-IR) spectroscopy using a Jasco FTIR-4100 Instrument in ATR mode. Finally, oxygenated groups were quantified by Boehm titrations with an automatic titrator Mettler-Toledo T70. Details of experimental conditions and procedures are described in previous work [26].

2.4. Batch incubations for the chemical transformation of iopromide

The abiotic reduction of IOP was assessed in batch incubations using MrGO-N and rGO-N as electron shuttles and sulfide as chemical electron donor (HS^- as the reactive species). These experiments were performed as previously proposed by Toral-Sánchez et al., [26] in the current study, 5 mg/L of MrGO-N or rGO-N as electron shuttle were used in a working volume of 50 mL. Experimental controls to verify stability and adsorption of IOP molecule were conducted simultaneously as previously described [26]. In order to monitor the removal of IOP and the chemical transformation byproducts during chemical reduction experiments, samples were analyzed at specific time intervals as described in section 2.5.

2.5. Analytical procedures

Measures of IOP concentration and identification of its chemical byproducts were performed by high-performance liquid chromatography (HPLC, Agilent Technology 1200 series chromatograph) and HPLC coupled to mass spectroscopy (HPLC-MS, Varian ® 500-MS ion trap mass spectrometer), respectively, using the experimental conditions indicated by Toral-Sánchez et al., [26].

3. Results and discussion

3.1. Characterization of graphene nanosacks

During the synthesis of GNS, the furnace temperature was 600 °C, converting the GO precursor to rGO-N by thermal reduction [28], which involves chemical and structural changes in the nanomaterials. In order to demonstrate the functionalization of MrGO-N with MNP, XRD analysis of this material was performed as shown in supplementary material (SM, Fig. 1S-a). Their XRD pattern shows typical peaks at 2θ = 18.29, 30.09, 35.44, 37.07, 43.07, 53.44, 56.96, 62.55, 74.00 and 89.65, which confirms the presence of MNP and suggests that the structure of encapsulated Fe_3O_4 particles were preserved during the aerosol processing. Also, Fig. 1S-b shows that MrGO-N can be separated from water solution with a magnet demonstrating the strong assembly of Fe_3O_4 nanoparticles in the GNS and the absence of rGO sheets dispersed in solution as previously reported by Chen et al., [28].

Micrographs of rGO-N are shown in Fig. 1A. Wrinkled GNS products with irregular folded nano-structures can be observed. According to Chen et al., the microdroplets drying time is around 0.1 to 100 ms [34], indicating that synthesis of these hybrid GNS was very fast. In addition, the mass ratio of water-GO suspension (2000:1) was estimated previously [34], suggesting that the encapsulation process involves a great size reduction of GO sheets, generating hybrid materials with nanometric size from aerosol suspended droplets [34]. Furthermore, Fig. 1B and C show high-resolution micrographs of MrGO-N. It can be seen in Fig. 1B a successful and almost completely assembly of MNP inside the sacks, with only few particles appearing on the external surface. Moreover, it can be observed in Fig. 1C that Fe_3O_4 nanoparticles were covered by partially rGO sheets. On the other hand, it has been reported a high stability (not unfold) of MrGO-N into water [34]. As mentioned by Chen et al., [28] the successful encapsulation and morphology of GNS are related to the electrostatic interactions that occurs in the Fe_3O_4/GO system.

Previous reports have proposed assembly mechanisms for hybrid GNS formation. Chen et al., [34] suggested, by molecular simulations, that GO sheets show a preference to adsorb at the air-water interface, forming rGO films that fold during droplet shrinkage external surface in the drying stage. Instead, the MNP prefer to be transported inside GNS by diffusion. In addition, the simulation analysis predict that the wrinkle locations of GNS are initiated from regions with high concentration of carbonyl and epoxy functionalities or defects in the GO sheets [34]. Moreover, Chen et al., [28] proposed a theory of nanoparticles encapsulation process in the sacks, which consist in the electrostatic attraction and repulsion behavior of GO/nanoparticles systems as a function of pH-dependent zeta potential. This theory establishes that the charged nanoparticles (with smaller size than GO sheets) have the ability

to diffuse from drying droplet external surface toward sack interior and then, charged GNS separation is performed by repulsive electrostatic interactions [28].

In this context, measurements of zeta potential as a function of pH for all nanomaterials were carried out (Fig. 2). It can be seen that GO has a point of zero charge (pH_{PZC}) of 2.3, in the range of carboxyl group pKa values, suggesting that these oxygenated groups are responsible of negative surface charge. The Fe_3O_4 nanoparticles show a pH_{PZC} of 6.9. The pH value of GO/Fe_3O_4 system was 3.2. At this pH, the MNP have a positive surface charge, which could interact with the negative charged of GO sheets by electrostatic interactions [28]. These results could explain the successful dispersion and assembly of magnetite in the GNS as observed in Fig. 1B and C. Moreover, it can be seen in Fig. 2 that the pH_{PZC} of precursor GO (pH=2.3) is lower with respect to the MrGO-N (pH=3.8), which indicates a partial reduction of GO sheets. Also, the pH_{PZC} of MrGO-N was slightly higher (pH=3.8) in comparison to rGO-N (pH=3.5), suggesting that a few MNP are exposed on the outer surface of MrGO-N, as shown in Fig. 1B.

On the other hand, it is possible to observe in Table 1 changes in surface chemical properties of hybrid GNS due to the partial thermal reduction of precursor GO sheets during the encapsulation process. The total concentration of acidic oxygenated groups decreased 25 % (from 3.04 to 2.28 milli-equivalents (meq)/g) as thermal reduction process of GO sheets is performed. Also, a slight increase on carbonyl groups was observed, from 1.05 to 1.20 meq/g. According to previous works, quinone groups have been suggested as a main electron shuttle moieties in carbon-based material due to its contribution in the reductive reactions of environmental contaminants [12,35]. Several studies have reported the possible mechanism involved in the thermal reduction of GO sheets. Accordingly, the energy required (binding energy) for bonds break between graphene sheets and different oxygenated groups could be a key factor in the thermal deoxygenation of GO [36], being the epoxy and carboxyl groups the easiest to remove at low temperature because of its chemical nature [37,38]. Also, Gao et al., [37] proposed that hydroxyl and carboxyl groups could be removed from GO sheets at the range of temperature between 100 to 600 °C. In contrast, carbonyl groups are highly stable and removed at critical temperatures above 1730 ° C. Moreover, Huh [39] proposed that during thermal reduction of GO, different stages of deoxygenation exist as the temperature increases. In this sense, the partial removal of carboxyl and hydroxyl groups, vaporization of H_2O, contraction of GO sheets and formation of CO and CO_2 occurs between room temperature and 600 °C. As can be seen in Table 1, carbonyl groups were less removed in comparison with hydroxyl and carboxyl groups, which corroborate the aforementioned.

The deoxygenation in the GNS was also confirmed by FT-IR spectroscopy. As shown in Fig. 3, all nanomaterials present the stretching vibration of O-H groups from 3000 to 3700 cm^{-1}. Also visible are bands corresponding to stretching vibrations of C-OH at 1200 cm^{-1}, C-O (epoxy groups) at 1040 cm^{-1} and C=O can be seen at 1720 cm^{-1} from carboxyl groups, respectively, which decreased after the thermal reduction of GO [15,26]. These observations agree with the quantification of oxygenated groups obtained by Boehm titrations (see Table 1). Furthermore, the appearance of aromatic C=C stretching vibration at 1620 cm^{-1} and the presence of C=O at 1570 from carbonyl groups [26] was also observed in the spectra of

MrGO-N and rGO-N. Finally, the MrGO-N spectrum shows a characteristic band at 585 cm $^{-1}$ corresponding to Fe-O stretching vibration from Fe_3O_4 nanoparticles [40]. These results demonstrate that hybrid GNS are formed with rGO sheets by thermal reduction process of GO precursor.

In order to characterize the evolution of GO precursor and crystallinity of GNS, Raman spectroscopy was employed. Fig. 4 shows Raman spectra of GO, rGO-N and MrGO-N. The presence of G and D bands at 1597 cm^{-1} and 1350 cm^{-1}, respectively, is evident. The D band is related to defects in the sp2-carbon network, indicating the amorphous character of materials. In contrast, the G band derived from vibrations within the defect-free sp2-carbon network [41]. Structural modifications in GNS can results from thermal reduction of precursor GO due to the reduction of oxygenated functionalities, which was confirmed by Raman spectra of MrGO-N and rGO-N. It can be seen that the relative intensity of the D band decreased and that of the G band increased as the synthesis of the GNS was conducted. Moreover, it has been reported that the structural disorder of carbon-based materials depends of the width of band D and the height of intermediate band A located between the D and G bands, which are related with the defects in the aromatic ring network of graphene sheet, specially for the presence of pentagon and heptagon carbon rings [42,43]. Accordingly, these results suggest that GO precursor undergoes a thermal reduction by heating indicating that synthesized GNS are formed by rGO sheets.

3.2. Chemical reduction of IOP

The chemical reduction of IOP by reaction with HS^- species along with experimental controls are shown in Fig. 5. Sulfide cases a decrease in IOP concentration with removal efficiencies of 57 and 72 % after 10 days, experiments involving rGO-N and MrGO-N, respectively. In contrast, low efficiency removal of IOP (25 %) was observed in control experiments without electron shuttle (direct reduction by sulfide). IOP adsorption controls (without sulfide as electron donor) showed a slight decrease on IOP concentration (< 12 % in all cases). Also, good stability of IOP molecule was observed in basal medium, showing a removal lower than 5 %.

Furthermore, the maximum removal rate calculated in chemical incubations conducted with MrGO-N and rGO-N were 57.73 and 38.91 μg/L-d, respectively. Meanwhile, the maximum removal rate achieved was only 22.58 μg/L-d in the control experiment lacking nanosacks as electron shuttle. These results represent a 2.5 and 1.7-fold increase in the maximum removal rate of IOP in the presence of MrGO-N and rGO-N, respectively, which suggest that the redox activity of MrGO-N as electron shuttle promoted the removal rate and reduction efficiency of IOP [27]. In the following section, it will be explored the molecular pathways involved in the chemical transformation of IOP.

3.3 Chemical transformation pathway of IOP

Previous studies have elucidated the chemical and biological transformation pathway of IOP using GO and rGO as electron shuttle under anaerobic conditions [26,27]. However, the abiotic transformation pathways have not been studied for IOP or any other recalcitrant pollutant using hybrid graphene nanosacks as electron shuttle. Samples from incubations

using MrGO-N as electron shuttle were analyzed by HPLC-MS with the aim to identify the chemical byproducts of IOP at specific time intervals during reduction experiments and propose a precise chemical transformation pathway of this pollutant. The molecular weights (*m/z*) of 12 transformation products (TPs) were identified. The elemental composition and suggested chemical structures of the TPs are shown in Fig. 6, which uses the time-dependent data to sketch the main chemical transformation pathways. Each TP and the reductive reactions that involve their structure modification are briefly described as follows.

The structure of TP 730.85, appearing in the 24 h (day 1) sample, indicates decarboxylation and deacetylation reactions in side chain B. In the day 2 sample, five further transformation products from TP 730.8 were observed. The structure of TP 729.90 and 714.50 implies a slight modification in side chain A, which includes dehydration and demethylation reactions. TP 662.70 indicates an N-demethylation in side chain A, decarboxylation and cleavage of the C-N and amide bonds at the side chain B. The rupture of side chain B, N-demethylation and cleavage of the C-N bond at the side chain A with subsequent removal of two iodine atoms (dehalogenation) of the aromatic ring results in the generation of TP 316.80. TP 248.90 involves the rupture of C-N bond in side chain B and deiodination of the aromatic ring (HI). After 4 days of incubation, two new chemical byproducts were generated from the original IOP molecule. TP 772.80 and 758.60 involve the loss of a molecule of H_2O in side chain A and B and sequential demethylation in side chain B. Also, TPs identified with *m/z* of 656.50 and 322.70 comes from either TP 729.90 or 714.50 after 6 days of incubation. TP 656.50 involves dehydration and demethylation reactions in side chain A and C-N bond rupture in side chain B. The cleavage of C-N bond and N-demethylation in side chain A, rupture of side chain B, demethylation and dehydration in side chain C and subsequent dehalogenation (removal of two iodine atoms) of the aromatic ring results in the formation of TP 322.70. Finally, the structure of TP 588.70 and 742.70 (generated after 8 days of incubation) represents a modification in side chain A and B of TP 772.80 and 758.60, respectively, which include demethylation, N-demethylation, dehydration and deiodination reactions. After 10 days of incubation, generation of new chemical byproducts was not observed. The mechanisms of the reductive transformation pathway and *m/z* of TPs proposed in this work are consistent with studies using other catalysts, reducing agents and degradation strategies [2,26,27,44–48].

Moreover, results previously obtained from assays carried out without electron shuttle (direct reduction by sulfide) revealed that the main TPs produced were 646.9, 768.7 and 788.8.[26] In consequence, it can be suggested that the redox catalytic activity of MrGO-N promoted reductive transformation reactions of IOP. This is supported by the generation of chemical byproducts with lower molecular weight as compared with TPs identified in control experiments conducted without MrGO-N (direct reduction of IOP by sulfide). Moreover, it can be observed that the TP with lowest *m/z* (248.90) was generated during the first 48 h. In addition, the complete deiodination of IOP molecule occurred at the same incubation time as can be seen in TP 248.90. These observations suggest that MrGO-N stimulated a greater transformation degree of IOP. The degradation of IOP and its correlation with the catalytic activity of MrGO-N can be elucidated by physicochemical properties of these hybrid nanomaterials as mentioned below.

3.4. Mechanism of IOP transformation mediated by MrGO-N

Different studies have explored the catalytic properties of carbon-based materials (e.g. activated carbon [20,49] carbon nanotubes [24,50] and activated carbon fibers [32,51]) in the degradation of persistent contaminants [27,49] due to the presence of quinone groups in their structure, which serve as electron shuttle [12]. As exposed by titration results (see Table 1, section 3.1), the MrGO-N have a higher percentage (12.5 % more) of quinone groups, which might satisfactorily explain the transformation degree and removal efficiency of IOP since these oxygenated groups have great catalytic activity [12,35]. These facts suggest that the redox activity of quinone-hydroquinone couples plays a fundamental role in the reductive degradation mechanisms of IOP due to its contribution in the electron transfer process.

Other potential transformation mechanism of IOP is reported in previous works [26,27,52], which involves the chemical association of reactive non-bonding π-electrons present at the edges of graphene sheets of MrGO-N with the hydrogen, hydroxyl and halogenated (iodinated) substituents of IOP molecule, promoting reductive reactions of this contaminant. This mechanism is supported by the generation of chemical transformation byproducts (partial rupture) of IOP as observed in the transformation pathway (see Fig. 6).

On the other hand, our previous work reported the chemical transformation of IOP in chemical assays with the use of rGO-based material as electron shuttles and sulfide as electron donor [26]. The results indicated an IOP removal efficiency of 66 % when rGO-4 material was applied as redox catalyst [26]. In comparison, the results obtained in this study (see section 3.2) showed an IOP removal efficiency of 77 % in the presence of MrGO-N as electron shuttle, indicating that the use of these nanomaterials further enhanced the reduction of IOP in chemical assays. In addition, the transformation pathways of IOP proposed in our previous work [26] and in the present research revealed important differences in the chemical structure of generated byproducts. For instance, the simplest chemical byproduct identified in experiments conducted with rGO-4 as redox catalysts was TP 314.18, indicating the removal of two iodine atoms (dehalogenation) and rupture of side chain A of the IOP molecule [26]. Meanwhile, the simplest structure identified in the experiments conducted with MrGO-N as redox catalyst was TP 248.90 (see section 3.3), suggesting the completely reductive dehalogenation (removal of three iodine atoms) and partial rupture of side chain A and B of the aromatic ring of IOP. These results exhibit that the presence of MrGO-N promoted a greater transformation degree of IOP in comparison with the experiments amended with rGO-4 material due to the presence of MNP immobilized in MrGO-N. Also, these facts suggest that the mechanisms involved in the reductive transformation of IOP are more complex in the presence of MrGO-N than in the presence of rGO-based materials as redox catalysts, which indicates important differences with what has been previously reported, contributing to scientific knowledge about the redox properties of hybrid graphene composites.

Consequently, it is possible to suggest that the presence of MNP (discussed in section 3.1) could be involved in the reductive reactions and transformation mechanism of IOP. Several studies have employed the reducing catalytic power of MNP in order to improve the reduction of halogenated pollutants, dyes and heavy metals [30,53]. Magnetite (Fe_3O_4) is an

iron oxide containing ferrous (Fe^{2+}) and ferric (Fe^{3+}) species in its chemical structure [54], which make it a potent reducing agent due to the redox processes that involve the reduction/oxidation of couple Fe^{2+}/Fe^{3+} [55]. In addition, magnetite has the ability to transfer electrons because of its elevated conductivity by electron hopping between Fe^{2+} and Fe^{3+} ions [54,56]. Accordingly, a mechanism for the reductive transformation of IOP implies that the redox activity of MNP (oxidation of Fe^{2+}) immobilized on the MrGO-N could transfer electrons to quinone groups of graphene sheets of nanosacks and then to IOP molecule, which is the final electron acceptor in the redox conversion process [30]. Also, a direct electron transfer from couple Fe^{2+}/Fe^{3+} redox activity toward IOP molecule may occur. As discussed in section 3.2, the reduction kinetics performed in the presence of MrGO-N showed a higher IOP removal efficiency than rGO-N (72 % compared to 57 %), which demonstrated that the presence of the Fe_3O_4 nanoparticles contribute in the electron transfer process for the degradation of IOP [30]. Based on the above, it can be concluded that the reductive transformation of IOP involves several mechanisms in the electron transfer process.

4. Conclusion

The novel and successful application of MrGO-N as redox catalysts is reported for the reductive transformation of IOP. The results obtained in this study demonstrated that the catalytic activity of MrGO-N enhances the removal and chemical transformation degree of IOP, showing an important contribution of chemical and physical properties of MrGO-N in the electron transfer process toward the electron-accepting pollutant, IOP. The physicochemical properties of rGO sheets that form the external surface of MNS were key factors in the chemical transformation of IOP due to its high electrical conductivity, chemical reactivity, and redox catalytic activity of quinone-hydroquinone couples. On the other hand, the few MNP exposed on the outer surface of MrGO-N also contributed in the reductive transformation of IOP by the rapid electron transfer and redox activity of couple Fe^{2+}/Fe^{3+} ions. These facts suggest that the great redox catalytic activity of MrGO-N was due to the synergy between redox properties of rGO sheets and MNP, indicating that several mechanisms are involved in the degradation of this persistent pollutant.

In comparison with rGO-based materials as electron shuttles, the MrGO-N increased the reduction and transformation degree of IOP, making the redox conversion process of this pollutant more complex and different from what has been previously reported. The reductive transformation pathway of IOP was proposed. Chemical transformation byproducts with lower molecular weight than IOP were identified, involving complete deiodinated of aromatic ring and partial rupture of ramifications of IOP molecule. Derived from this study, new challenges are focused on designing a system to retain MrGO-N as redox catalyst in a continuous biological system to promote the reductive biodegradation of recalcitrant pollutants from water.

Supplementary Material

Refer to Web version on PubMed Central for supplementary material.

Acknowledgements

This work was financially supported by grants from the Council of Science and Technology of Mexico (Grants SEP-CB-2014–237118 and 1289 of the Frontiers of Science program), the Marcos Moshinsky Foundation and the Superfund Research Program of the National Institute of Environmental Health Sciences, grant 2P42 ES013660. The authors also appreciate the help provided by national laboratories LANBAMA and LINAN from IPICYT for its help with the samples analysis. Finally, Toral-Sánchez thanks the scholarship received from CONACYT (378326), as well as the technical support of A. Colunga-Álvarez, D. Partida-Gutiérrez, G. Vidriales-Escobar, J.P. Rodas-Ortiz, Ma. del C. Rocha-Medina, B. Rivera-Escoto, Z. Saleeba and R. Torasso.

References

[1]. Knitt LE, Shapley JR, Strathmann TJ, Rapid metal-catalyzed hydrodehalogenation of iodinated x-ray contrast media, Environ. Sci. Technol 42 (2008) 577–583. doi:10.1021/es071837y. [PubMed: 18284165]

[2]. Schulz M, Löffler D, Wagner M, Ternes TA, Transformation of the X-ray contrast medium iopromide in soil and biological wastewater treatment, Environ. Sci. Technol 42 (2008) 7207–7217. doi:10.1021/es800789r. [PubMed: 18939548]

[3]. Onesios KM, Yu JT, Bouwer EJ, Biodegradation and removal of pharmaceuticals and personal care products in treatment systems: a review, Biodegradation 20 (2009) 441–466. doi:10.1007/s10532-008-9237-8. [PubMed: 19112598]

[4]. Ternes TA, Hirsch R, Occurrence and behavior of X-ray contrast media in sewage facilities and the aquatic environment, Environ. Sci. Technol 34 (2000) 2741–2748. doi:10.1021/es991118m.

[5]. Busetti F, Linge KL, Rodriguez C, Heitz A, Occurrence of iodinated X-ray contrast media in indirect potable reuse systems, J. Environ. Sci. Health Part A Tox. Hazard. Subst. Environ. Eng 45 (2010) 542–548. doi:10.1080/10934521003595100.

[6]. Putschew A, Wischnack S, Jekel M, Occurrence of triiodinated X-ray contrast agents in the aquatic environment, Sci. Total Environ 255 (2000) 129–134. doi:10.1016/S0048-9697(00)00461-7. [PubMed: 10898400]

[7]. Steger-Hartmann T, Länge R, Schweinfurth H, Environmental risk assessment for the widely used iodinated X-ray contrast agent iopromide (Ultravist), Ecotoxicol. Environ. Saf 42 (1999) 274–281. doi:10.1006/eesa.1998.1759. [PubMed: 10090816]

[8]. Peer A, Averbukh Z, Berman S, Modai D, Averbukh M, Weissgarten J, Contrast media augmented apoptosis of cultured renal mesangial, tubular, epithelial, endothelial, and hepatic cells, Invest. Radiol 38 (2003) 177–182. doi:10.1097/01.RLI.0000054529.61167.84. [PubMed: 12595799]

[9]. Zhao Y, Tao Z, Xu Z, Tao Z, Chen B, Wang L, Li C, Chen L, Jia Q, Jia E, Zhu T, Yang Z, Toxic effects of a high dose of non-ionic iodinated contrast media on renal glomerular and aortic endothelial cells in aged rats in vivo, Toxicol. Lett 202 (2011) 253–260. doi:10.1016/j.toxlet.2011.02.011. [PubMed: 21354280]

[10]. Kwon M, Yoon Y, Cho E, Jung Y, Lee B-C, Paeng K-J, Kang J-W, Removal of iopromide and degradation characteristics in electron beam irradiation process, J. Hazard. Mater 227–228 (2012) 126–134. doi:10.1016/j.jhazmat.2012.05.022.

[11]. Bottinor W, Polkampally P, Jovin I, Adverse reactions to iodinated contrast media, Int. Coll. Angiol. Inc 22 (2013) 149–154. doi:10.1055/s-0033-1348885.

[12]. Leon CA Leon y D, Radovic LR, Interfacial chemistry and electrochemistry of carbon surfaces, in: Chem. Phys. Carbon, Marcel Dekker, New York, 1994: pp. 227–405.

[13]. van der Zee FP, Cervantes FJ, Impact and application of electron shuttles on the redox (bio)transformation of contaminants: A review, Biotechnol. Adv 27 (2009) 256–277. doi:10.1016/j.biotechadv.2009.01.004. [PubMed: 19500549]

[14]. Guin PS, Das S, Mandal PC, Electrochemical reduction of quinones in different media: a review, Int. J. Electrochem 2011 (2011) 1–22. doi:10.4061/2011/816202.

[15]. Geim AK, Graphene: status and prospects, Science 324 (2009) 1530–1534. doi:10.1126/science.1158877. [PubMed: 19541989]

[16]. Enoki T, Kobayashi Y, Katsuyama C, Osipov VY, Baidakova MV, Takai K, Fukui K, Vul AY, Structures and electronic properties of surface/edges of nanodiamond and nanographite, Diam. Relat. Mater 16 (2007) 2029–2034. doi:10.1016/j.diamond.2007.07.024.

[17]. Dreyer DR, Park S, Bielawski CW, Ruoff RS, The chemistry of graphene oxide, Chem. Soc. Rev 39 (2009) 228–240. doi:10.1039/B917103G. [PubMed: 20023850]

[18]. Fu H, Zhu D, Graphene oxide-facilitated reduction of nitrobenzene in sulfide-containing aqueous solutions, Environ. Sci. Technol 47 (2013) 4204–4210. doi:10.1021/es304872k. [PubMed: 23561007]

[19]. Cervantes FJ, van der Velde S, Lettinga G, Field JA, Quinones as terminal electron acceptors for anaerobic microbial oxidation of phenolic compounds, Biodegradation 11 (2000) 313–321. [PubMed: 11487061]

[20]. Pereira RA, Pereira MFR, Alves MM, Pereira L, Carbon based materials as novel redox mediators for dye wastewater biodegradation, Appl. Catal. B Environ 144 (2014) 713–720. doi: 10.1016/j.apcatb.2013.07.009.

[21]. Savaram K, Li M, Tajima K, Takai K, Hayashi T, Hall G, Garfunkel E, Osipov V, He H, Dry microwave heating enables scalable fabrication of pristine holey graphene nanoplatelets and their catalysis in reductive hydrogen atom transfer reactions, Carbon 139 (2018) 861–871. doi: 10.1016/j.carbon.2018.07.047.

[22]. Colunga A, Rangel-Mendez JR, Celis LB, Cervantes FJ, Graphene oxide as electron shuttle for increased redox conversion of contaminants under methanogenic and sulfate-reducing conditions, Bioresour. Technol 175 (2015) 309–314. doi:10.1016/j.biortech.2014.10.101. [PubMed: 25459837]

[23]. Lu H, Zhang H, Wang J, Zhou J, Zhou Y, A novel quinone/reduced graphene oxide composite as a solid-phase redox mediator for chemical and biological Acid Yellow 36 reduction, RSC Adv 4 (2014) 47297–47303. doi:10.1039/C4RA08817D.

[24]. Fu H, Guo Y, Chen W, Gu C, Zhu D, Reductive dechlorination of hexachloroethane by sulfide in aqueous solutions mediated by graphene oxide and carbon nanotubes, Carbon 72 (2014) 74–81. doi:10.1016/j.carbon.2014.01.053.

[25]. Li L, Liu Q, Wang Y-X, Zhao H-Q, He C-S, Yang H-Y, Gong L, Mu Y, Yu H-Q, Facilitated biological reduction of nitroaromatic compounds by reduced graphene oxide and the role of its surface characteristics, Sci. Rep 6 (2016) 30082. doi:10.1038/srep30082. [PubMed: 27439321]

[26]. Toral-Sánchez E, Valdés J.A. Ascacio, Aguilar CN, Cervantes FJ, Rangel-Mendez JR, Role of the intrinsic properties of partially reduced graphene oxides on the chemical transformation of iopromide, Carbon 99 (2016) 456–465. doi:10.1016/j.carbon.2015.12.067.

[27]. Toral-Sánchez E, Rangel-Mendez JR, Valdés J.A. Ascacio, Aguilar CN, Cervantes FJ, Tailoring partially reduced graphene oxide as redox mediator for enhanced biotransformation of iopromide under methanogenic and sulfate-reducing conditions, Bioresour. Technol 223 (2017) 269–276. doi:10.1016/j.biortech.2016.10.062. [PubMed: 27969578]

[28]. Chen Y, Guo F, Qiu Y, Hu H, Kulaots I, Walsh E, Hurt RH, Encapsulation of particle ensembles in graphene nanosacks as a new route to multifunctional materials, ACS Nano 7 (2013) 3744–3753. doi:10.1021/nn3055913. [PubMed: 23560523]

[29]. Panich AM, Shames AI, Tsindlekht MI, Osipov VY, Patel M, Savaram K, He H, Structure and magnetic properties of pristine and Fe-doped micro- and nanographenes, J. Phys. Chem. C 120 (2016) 3042–3053. doi:10.1021/acs.jpcc.5b11732.

[30]. Pereira L, Dias P, Soares OSGP, Ramalho PSF, Pereira MFR, Alves MM, Synthesis, characterization and application of magnetic carbon materials as electron shuttles for the biological and chemical reduction of the azo dye Acid Orange 10, Appl. Catal. B Environ 212 (2017) 175–184. doi:10.1016/j.apcatb.2017.04.060.

[31]. Lv XS, Qiu Y, Wang ZY, Jiang GM, Chen YT, Xu XH, Hurt RH, Aerosol synthesis of phase-controlled iron–graphene nanohybrids through FeOOH nanorod intermediates, Environ. Sci. Nano 3 (2016) 1215–1221. doi:10.1039/C6EN00178E. [PubMed: 28133538]

[32]. Amezquita-Garcia HJ, Razo-Flores E, Cervantes FJ, Rangel-Mendez JR, Activated carbon fibers as redox mediators for the increased reduction of nitroaromatics, Carbon 55 (2013) 276–284. doi: 10.1016/j.carbon.2012.12.062.

[33]. Guo F, Silverberg G, Bowers S, Kim S-P, Datta D, Shenoy V, Hurt RH, Graphene-based environmental barriers, Environ. Sci. Technol 46 (2012) 7717–7724. doi:10.1021/es301377y. [PubMed: 22717015]

[34]. Chen Y, Guo F, Jachak A, Kim S-P, Datta D, Liu J, Kulaots I, Vaslet C, Jang HD, Huang J, Kane A, Shenoy VB, Hurt RH, Aerosol synthesis of cargo-filled graphene nanosacks, Nano Lett 12 (2012) 1996–2002. doi:10.1021/nl2045952. [PubMed: 22429091]

[35]. Montes-Morán MA, Suárez D, Menéndez JA, Fuente E, On the nature of basic sites on carbon surfaces: an overview, Carbon 42 (2004) 1219–1225. doi:10.1016/j.carbon.2004.01.023.

[36]. Pei S, Cheng H-M, The reduction of graphene oxide, Carbon 50 (2012) 3210–3228. doi:10.1016/j.carbon.2011.11.010.

[37]. Gao X, Jang J, Nagase S, Hydrazine and thermal reduction of graphene oxide: reaction mechanisms, product structures, and reaction design, J. Phys. Chem. C 114 (2010) 832–842. doi:10.1021/jp909284g.

[38]. Bagri A, Mattevi C, Acik M, Chabal YJ, Chhowalla M, Shenoy VB, Structural evolution during the reduction of chemically derived graphene oxide, Nat. Chem 2 (2010) 581–587. doi:10.1038/nchem.686. [PubMed: 20571578]

[39]. Huh SH, Thermal reduction of graphene oxide, Phys. Appl. Graphene InTechOpen (2011) 73–90. doi:10.5772/14156.

[40]. Maity D, Kale SN, Kaul-Ghanekar R, Xue J-M, Ding J, Studies of magnetite nanoparticles synthesized by thermal decomposition of iron (III) acetylacetonate in tri(ethylene glycol), J. Magn. Magn. Mater 321 (2009) 3093–3098. doi:10.1016/j.jmmm.2009.05.020.

[41]. Wang G, Yang J, Park J, Gou X, Wang B, Liu H, Yao J, Facile synthesis and characterization of graphene nanosheets, J. Phys. Chem. C 112 (2008) 8192–8195. doi:10.1021/jp710931h.

[42]. Bogdanov K, Fedorov A, Osipov V, Enoki T, Takai K, Hayashi T, Ermakov V, Moshkalev S, Baranov A, Annealing-induced structural changes of carbon onions: High-resolution transmission electron microscopy and Raman studies, Carbon 73 (2014) 78–86. doi:10.1016/j.carbon.2014.02.041.

[43]. Mykhailiv O, Zubyk H, Plonska-Brzezinska ME, Carbon nano-onions: Unique carbon nanostructures with fascinating properties and their potential applications, Inorganica Chim. Acta 468 (2017) 49–66. doi:10.1016/j.ica.2017.07.021.

[44]. Pat-Espadas AM, Razo-Flores E, Rangel-Mendez JR, Ascacio-Valdes JA, Aguilar CN, Cervantes FJ, Immobilization of biogenic Pd(0) in anaerobic granular sludge for the biotransformation of recalcitrant halogenated pollutants in UASB reactors, Appl. Microbiol. Biotechnol (2015) 1–10. doi:10.1007/s00253-015-7055-6.

[45]. Cruz-Zavala AS, Pat-Espadas AM, Rangel-Mendez JR, Chazaro-Ruiz LF, Ascacio-Valdes JA, Aguilar CN, Cervantes FJ, Immobilization of metal–humic acid complexes in anaerobic granular sludge for their application as solid-phase redox mediators in the biotransformation of iopromide in UASB reactors, Bioresour. Technol 207 (2016) 39–45. doi:10.1016/j.biortech.2016.01.125. [PubMed: 26868154]

[46]. Gros M, Cruz-Morato C, Marco-Urrea E, Longrée P, Singer H, Sarrà M, Hollender J, Vicent T, Rodriguez-Mozaz S, Barceló D, Biodegradation of the X-ray contrast agent iopromide and the fluoroquinolone antibiotic ofloxacin by the white rot fungus Trametes versicolor in hospital wastewaters and identification of degradation products, Water Res 60 (2014) 228–241. doi:10.1016/j.watres.2014.04.042. [PubMed: 24867600]

[47]. Eversloh C. Lütke, Henning N, Schulz M, Ternes TA, Electrochemical treatment of iopromide under conditions of reverse osmosis concentrates – Elucidation of the degradation pathway, Water Res 48 (2014) 237–246. doi:10.1016/j.watres.2013.09.035. [PubMed: 24140349]

[48]. Pérez S, Eichhorn P, Celiz MD, Aga DS, Structural characterization of metabolites of the X-ray contrast agent iopromide in activated sludge using ion trap mass spectrometry, Anal. Chem 78 (2006) 1866–1874. doi:10.1021/ac0518809. [PubMed: 16536422]

[49]. van der Zee FP, Bisschops IAE, Lettinga G, Field JA, Activated carbon as an electron acceptor and redox mediator during the anaerobic biotransformation of azo dyes, Environ. Sci. Technol 37 (2003) 402–408. doi:10.1021/es025885o. [PubMed: 12564915]

[50]. Chen W, Zhu D, Zheng S, Chen W, Catalytic effects of functionalized carbon nanotubes on dehydrochlorination of 1,1,2,2-Tetrachloroethane, Environ. Sci. Technol 48 (2014) 3856–3863. doi:10.1021/es405683d. [PubMed: 24617768]

[51]. Toro E. Emilia Rios-Del, Celis LB, Cervantes FJ, Rangel-Mendez JR, Enhanced microbial decolorization of methyl red with oxidized carbon fiber as redox mediator, J. Hazard. Mater 260 (2013) 967–974. doi:10.1016/j.jhazmat.2013.06.056. [PubMed: 23892163]

[52]. Jiang D, Sumpter BG, Dai S, The unique chemical reactivity of a graphene nanoribbon's zigzag edge, J. Chem. Phys 126 (2007) 134701. doi:10.1063/1.2715558. [PubMed: 17430050]

[53]. Gorski CA, Nurmi JT, Tratnyek PG, Hofstetter TB, Scherer MM, Redox behavior of magnetite: Implications for contaminant reduction, Environ. Sci. Technol 44 (2010) 55–60. doi:10.1021/es9016848. [PubMed: 20039733]

[54]. Scott TB, Allen GC, Heard PJ, Randell MG, Reduction of U(VI) to U(IV) on the surface of magnetite, Geochim. Cosmochim. Acta 69 (2005) 5639–5646. doi:10.1016/j.gca.2005.07.003.

[55]. White AF, Peterson ML, Reduction of aqueous transition metal species on the surfaces of Fe(II)-containing oxides, Geochim. Cosmochim. Acta 60 (1996) 3799–3814. doi:10.1016/0016-7037(96)00213-X.

[56]. Allen GC, Curtis MT, Hooper AJ, Tucker PM, X-Ray photoelectron spectroscopy of iron–oxygen systems, J. Chem. Soc. Dalton Trans 0 (1974) 1525–1530. doi:10.1039/DT9740001525.

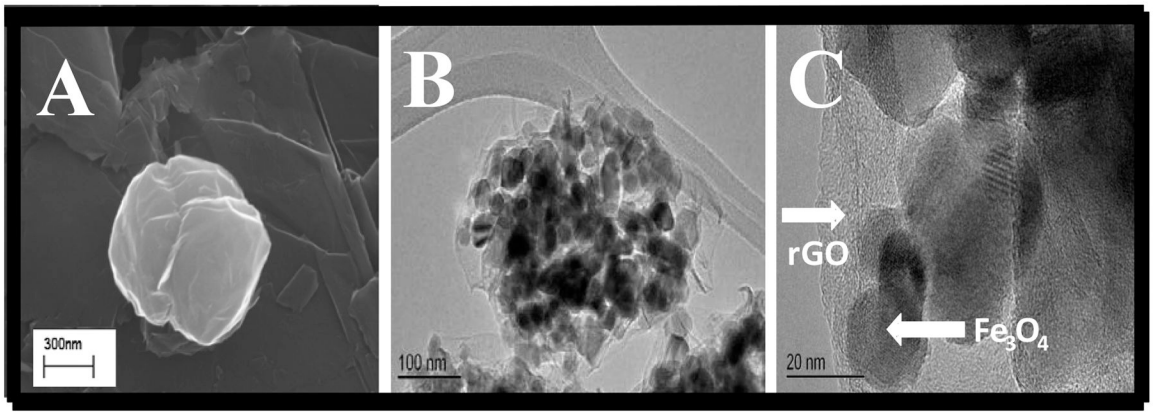

Figure 1.
SEM images of empty rGO-N (A). HR-TEM images of MrGO-N (B) and multilayer graphene sheets encapsulating MNP (C).

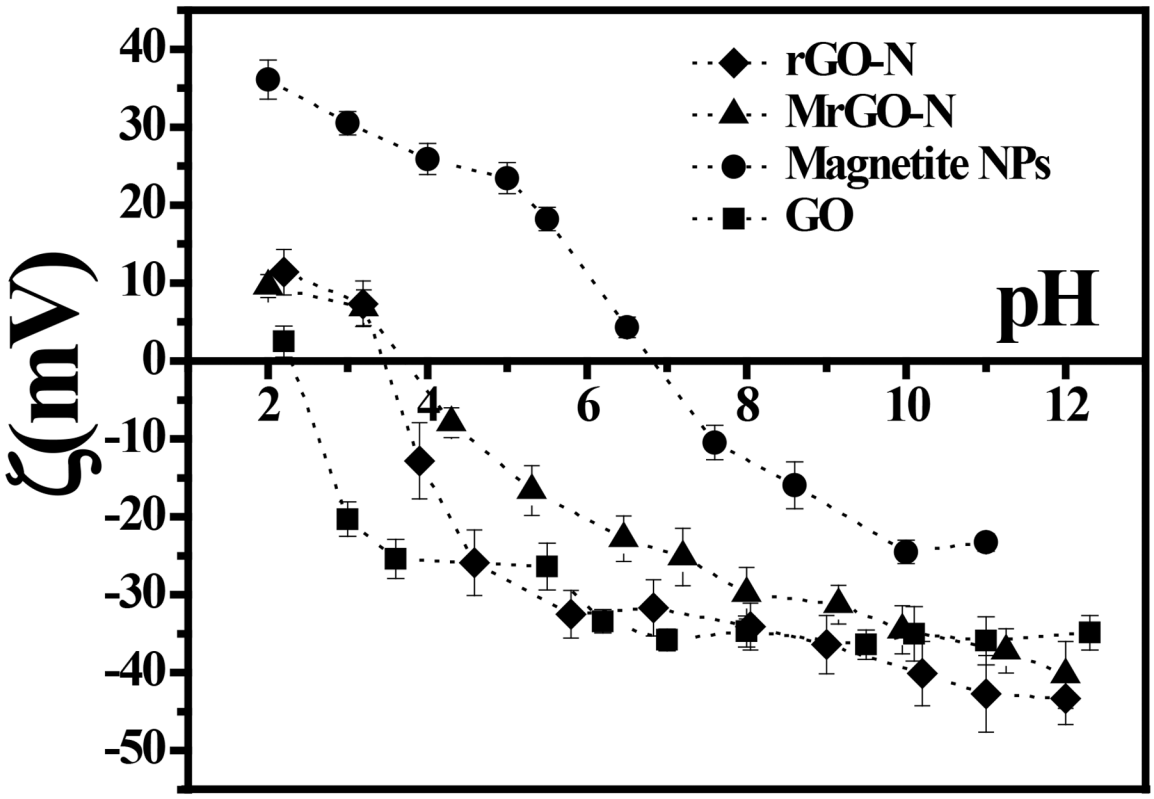

Figure 2.
Surface charge distribution of GO-based materials and MNP.

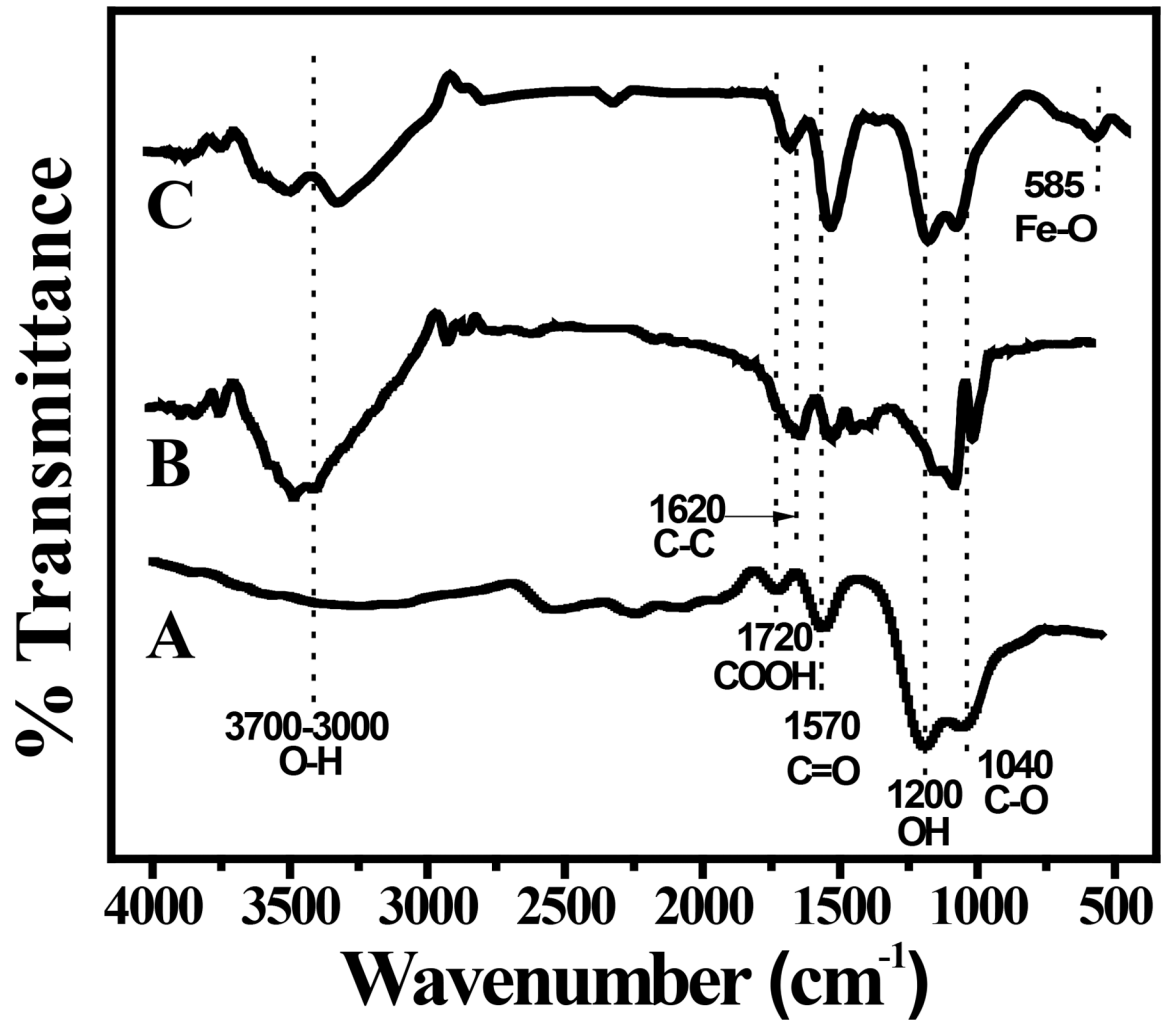

Figure 3.
FT-IR spectra of GO-based materials: (A) precursor GO, (B) rGO-N and (C) MrGO-N.

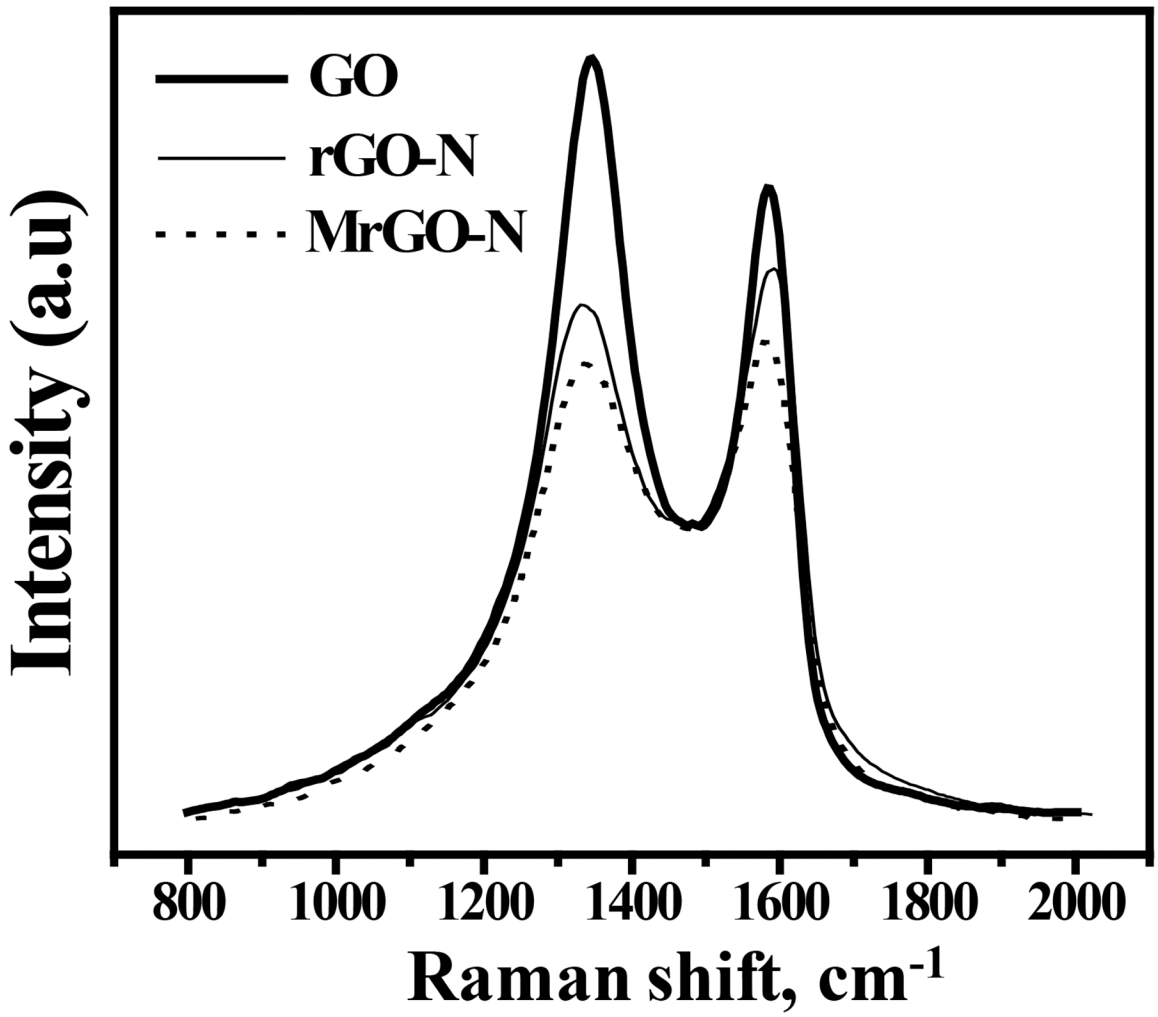

Figure 4.
Raman spectra of precursor GO, rGO-N and MrGO-N.

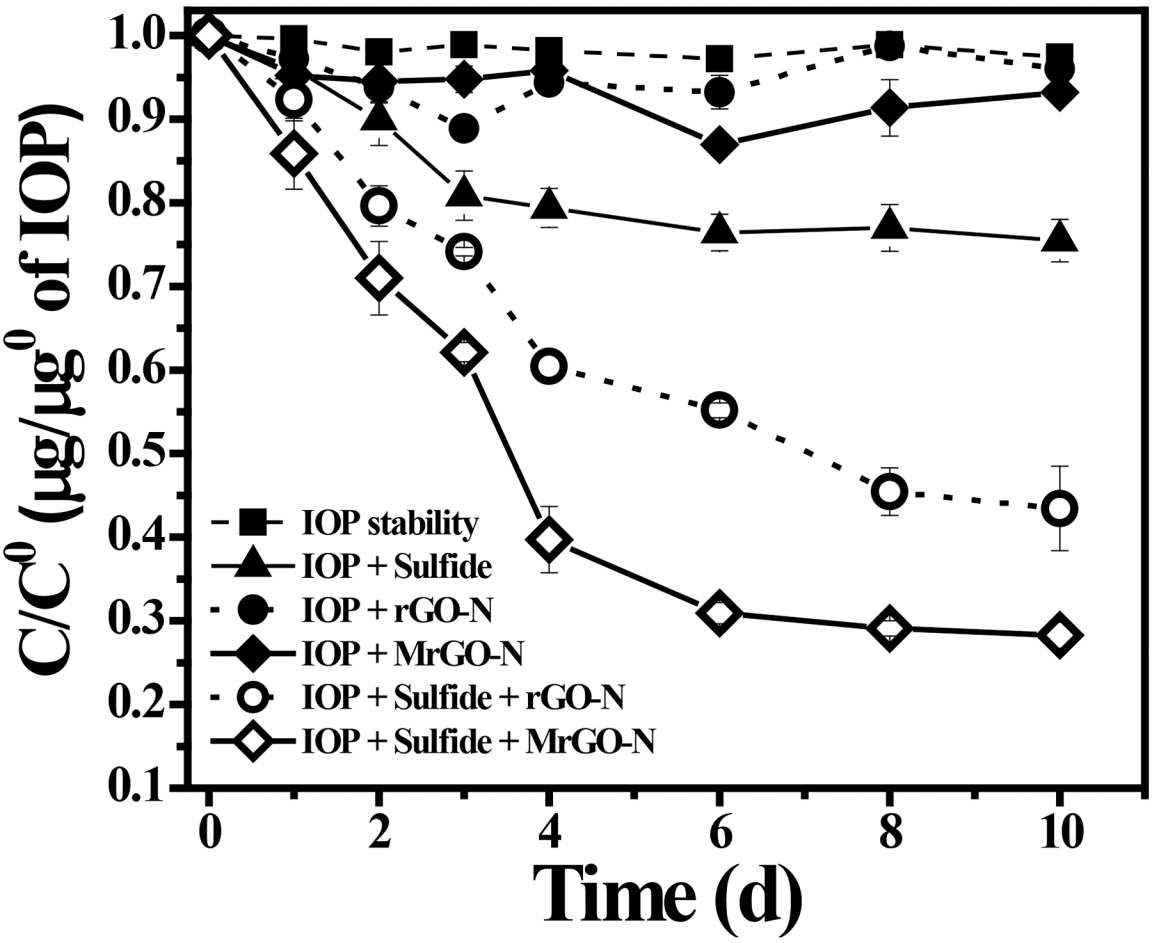

Figure 5.
GO-based materials catalysis of IOP reduction by sulfide. IOP stability control, direct chemical reduction control (IOP + Sulfide), adsorption controls (IOP + GO-based materials) and reduction experiments (IOP + Sulfide + GO-based materials) of rGO-N and MrGO-N.

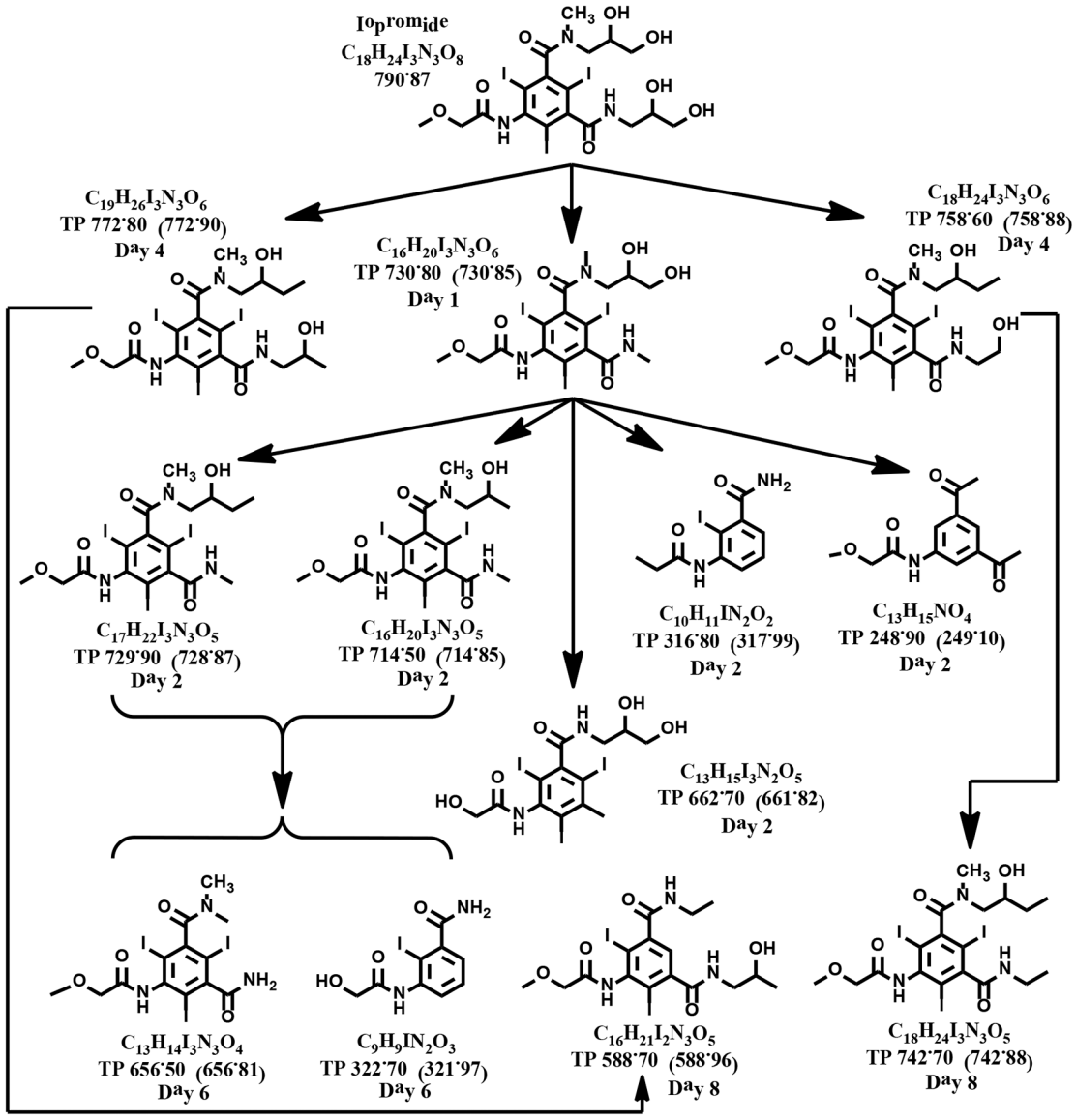

Figure 6.

Chemical transformation pathway of IOP and generation of byproducts through incubation time by MrGO-N as RM.

Table 1.

Surface chemical properties of precursor GO and MrGO-N.

	Surface functional groups, (meq/g)					Point of Zero Charge (pH_{PZC})
Samples	**Carboxylic**	**Lactonic**	**Phenolic**	**Carbonyl**	**Total**	
GO	1.62	0.20	0.17	1.05	3.04	2.30
MrGO-N	0.87	0.11	0.10	1.20	2.28	3.80